Green Tensor for a General Anisotropic Slip Condition

A. Sellier and N. Ghalia

Abstract: The Green tensor complying with *anisotropic* slip conditions at the surface of a plane, impermeable, motionless and slipping wall is theoretically obtained and an efficient numerical method is proposed to accurately compute at a very reasonable cpu time cost each of its Cartesian component. The accuracy of the advocated numerical strategy is tested against the Maple Software and the employed procedure makes it possible to calculate the Green tensor for a non-isotropic slip condition at a cpu time cost comparable with the one needed for the less complicated isotropic Navier condition.

Keywords: Stokes flow, plane wall, non-isotropic slip condition, Green tensor.

1 Introduction

It is well known that particle-particle and/or particle-boundary interactions strongly affect the macroscopic properties (such as effective viscosity) of a suspension made of solid particles immersed in a Newtonian liquid with uniform density ρ and viscosity μ. Of course, particle-boundary interactions close to a boundary deeply depend upon the boundary shape (plane, curved) and rouhgness. Today, one can elaborate surfaces with a selected roughness (using micro-scaled or nano-scaled patterns) or hydrophobicity at which the usual no-slip boundary condition is not valid any more and must be replaced with a so-called slip condition. Assuming henceforth a liquid flow with velocity $\mathbf{u}$ and pressure p above the motionless and impermeable $x_3 = 0$ plane boundary Σ and using Cartesian coordinates (O, x_1, x_2, x_3) with origin O attached to Σ, one therefore switch from the usual no-slip condition

$$u_i = \mathbf{u}.\mathbf{e}_i = 0 \quad \text{at } \Sigma(x_3 = 0) \text{ for } i = 1,2,3 \tag{1}$$

to another slip condition to be proposed in accordance with the experimental investigations. The widely-employed and well experimentally supported (see Churaev, Sobolev, and Somov (1994), Baudry, Charlaix, Tonck, and Mazuyer (2001)) one is the famous Navier (1823) slip condition

$$u_1 = b\frac{\partial u_1}{\partial x_3}, \; u_2 = b\frac{\partial u_2}{\partial x_3} \text{ and } u_3 = 0 \text{ at } \Sigma(x_3 = 0) \tag{2}$$

where $b > 0$ is the (effective) slip length and may be seen as the distance to which the velocity should be extrapolated inside the solid boundary to vanish. When compared with (1) the condition (2) clearly allows a non-zero tangential fluid velocity at the slipping (but still impermeable) motionless wall Σ. In addition, since it actually permits the liquid to slip with the same magnitude whatever the tangential direction the condition (2) is isotropic. However, by using anisotropic textures it is possible to produce patterned surfaces admitting properties depending upon the selected direction tangent to the surface. For these surfaces (2) is not valid any more and a non-istopic slip condition has been therefore recently proposed (see Stone, Stroock, and Adjari (2004), Bazant and Vinagradova (2008)). This condition distinguishes two othogonal tangential directions: the fastest one $\mathbf{e}_1$ with slip length $b_1 > 0$ and the slowest one $\mathbf{e}_2$ with slip length b_2 such that $0 < b_2 < b_1$. It then reads

$$u_1 = b_1 \frac{\partial u_1}{\partial x_3}, \ u_2 = b_2 \frac{\partial u_2}{\partial x_3} \text{ and } u_3 = 0 \text{ at } \Sigma(x_3 = 0). \tag{3}$$

Through adequate models it is possible to relate the slip lengths b_1 and b_2 to some of the surface pattern characteristics. In order to encompass usual boundary conditions (1)-(2) we henceforth assume that $b_1 \geq b_2 \geq 0$ in the adopted anisotropic slip condition (3).

We denote by a and V the flow typical length scale and velocity scale, respectively. For applications involving flows in micro-channels and/or suspensions made of micro-sized solid particles it turns out that $\text{Re} = \rho V a/\mu \ll 1$. In other words, inertial effects are negligible and in practice the flow $(\mathbf{u}, p)$ obeys the steady Stokes equations in the liquid domain. These equations are supplemented with relevant boundary conditions at infinity in each direction where the liquid domain is unbounded and additional conditions on each particle's surface and each boundary. Within this framework of Low-Reynolds-Number flow there is a considerable body of literature. Since this it not the aim of the present paper to review this huge literature we content ourselves with directing the reader to the well-established textbooks by Happel and Brenner (1991) and Kim and Karrila (1991) and aslo briefly distinguishing the employed procedures and associated advantages and drawbacks as follows:

(1) Analytical solutions. Exact solutions (available in previously-quoted textbooks and Feuillebois (1989)) exist for one spherical or ellipsoidal solid particle immersed in an unbounded liquid. These solutions, sometimes obtained by using a few carefully-selected singularities outside the liquid domain, provide excellent benchmark tests for the other procedures but are unfortunately restrited to quite a very few particle geometries and unbounded liquid domains.

(2) Semi-analytical solutions. These solutions are obtained using the so-called

bipolar coordinates which permit one to adress the case of two spherical particles in an unbounded liquid (see the pionnering work by Stimson and Jeffery (1926)) or one spherical particle interacting with a spherical cavity (see for instance Jones (2009)) or a plane impermeable wall (see Brenner (1961); Maude (1961); Dean and O'Neill (1963); O'Neill (1964, 1967, 1968); Cooley and O'Neill (1969); O'Neill (1969) where the no-slip condition holds. The case of a plane impermeable and slipping wall with anisotropic Navier condition (2) has also been treated in O'Neill and Bhatt (1991); Davis, Kezirian, and Brenner (1994); Feuillebois, Loussaief, and Pasol (2009) whereas references dealing with one or two bubbles or drops using the same approach are given in the review by Pasol, Sellier, and Feuillebois (2010). The bipolar coordinates provides accurate results but is by essence restricted to the case of one or two spherical particles (solid, bubble, droplet).

(3) The multipoles method. This approach, reviewed in Ekiel-Jeżewska and Wajnryb (2009), makes it possible to accurately deal with several interacting solid spheres as done in Cichocki, Felderhof, Hinsen, Wajnryb, and Bławzdziewicz (1994) and also spheres interacting with one (see Cichocki and Jones (1998), Cichocki, Jones, Kutteh, and Wajnryb (2000)) or two parallel plane and no-slipping wall(s) (see Jones (2004), Bhattacharya, Bławzdziewicz, and Wajnryb (2005)). Although this technique makes it possible to handle several spheres it is however restricted once more to spherical particles. One should also mention that the collocation point method employed in Hsu and Ganatos (1989, 1994) is similar to the multipoles method.

(4) The Boundary-integral method. This approach, theoretically studied in Ladyzhenskaya (1969) and seemingly first implemented by Youngren and Acrivos (1975, 1976), reduces the problem to the numerical treatment of a few boundary-integral equations. In contrast to other techniques it allows one to cope with arbitrarily-shaped particles. For a bounded liquid domain, it however becomes very cpu time consuming if the boundary-integral equation also involves the entire liquid boundary (which is in general the case). This drawback is in practice nicely circumvented as soon as one is able to obtain a so-called Green tensor (see the definition in §2.1) which however depends upon the encountered liquid boundaries. This Green tensor has been obtained for a a few no-slipping boundaries and the reader is directed to Lorenz (1907) and Blake (1971) for a plane wall with condition (1), to Oseen (1927) and Sellier (2008) for a spherical boundary, to Liron and Shahar (1978) for a liquid bounded by a circular pipe, to Miyazaki and Hasimoto (1978) for a plane boundary with a circular hole, to Liron and Mochon (1976) and Jones (2004) for two parallele plane walls. Note that the Green tensor for a liquid domain confined by a no-slippling plane wall and a parallel and free surface has also been determined in Sellier and Pasol (2006).

It turns out that the Boundary-integral method is a powerfool technique which actully also receives an efficient implementation for bounded Stokes flows as soon as the following two basic issues are adequately solved:

Issue 1: One is able to determine a so-called Green tensor which complies with the conditions to be satisfied by the flow on each boundary (except the particles surfaces).

Issue 2: One is able to quickly and accurately compute as many time as necessary the obtained Green tensor.

While Issue 1 is thus satisfied for the previously-quoted examples for which the Green tensor has been obtained one should note that, for example, Issue 2 has not yet been adequately adressed for the Green tensor obtained in Liron and Shahar (1978).

The aim of the present work is to determine the Green tensor associated with the general anisotropic slip condition (3) and also to present an efficient numerically strategy to accurately calculate its Cartesian components at a reasonable cpu time. The paper is organized as follows. The governing problem for the Green tensor and some key remarks motivating its introduction are given in §2 whereas the determination of the Green tensor is addressed in §3. An efficient numerical strategy to accurately compute each Cartesian component of the obtained Green tensor is proposed and benchmarked against the Maple Software in §4. Finally, a few remarks in §5 close the paper.

2   Green tensor: governing problem and motivations

This section defines the Green tensor for Stokes flows in the half $x_3 > 0$ space and subject to the anisotropic slip condition (3) on the plane $x_3 = 0$ impermeable and motionless boundary Σ. It also illustrates the use of this Green tensor by proposing a relevant boundary-integral equation to determine the Stokes flow about a single solid particle immersed in the liquid in the vicinity of the surface Σ and experiencing a prescribed rigid-body migration.

2.1   *Definition of the Green tensor and basic symmetry property*

Let us consider, as sketched in Fig. 1, two points located in the liquid domain above the plane boundary Σ : one so-called source point **y** and the observation point **x**. We also recall that Cartesian coordinates (O, x_1, x_2, x_3) are employed with $x_i = \mathbf{x}.\mathbf{e}_i$ and $y_i = \mathbf{x}.\mathbf{e}_i$.

For $k = 1, 2, 3$ we can introduce a Stokes flow with pressure $p^{(k)}$, velocity $\mathbf{v}^{(k)}$ produced by a concentrated point force with strength $\mathbf{e}_k$ placed at the source **y**.
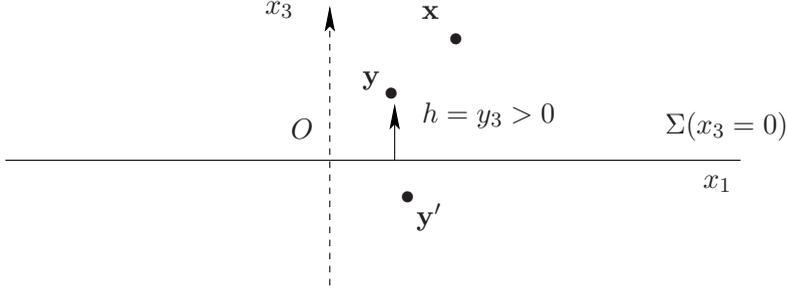
Figure 1: A pole **y** and its symmetric **y'** with respect to the plane wall $\Sigma(x_3 = 0)$.

This flow vanishes far from the source **y**. Accordingly, one has

$$\mu \nabla^2 \mathbf{v}^{(k)} = \nabla p^{(k)} - \delta_{3d}(\mathbf{x} - \mathbf{y})\mathbf{e}_k \quad \text{for } x_3 > 0, \tag{4}$$

$$\nabla . \mathbf{v}^{(k)} = 0 \quad \text{for } x_3 > 0, \tag{5}$$

$$(\mathbf{u}^{(k)}, p^{(k)}) \to (\mathbf{0}, 0) \quad \text{as } |\mathbf{x}| \to \infty \tag{6}$$

with $\delta_{3d}(\mathbf{x} - \mathbf{y}) = \delta_d(x_1 - y_1)\delta_d(x_2 - y_2)\delta_d(x_3 - y_3)$ if δ_d denotes the usual Dirac pseudo-function. The previous flows introduce a second-rank Green tensor **G** with Cartesian components $G_{jk}(\mathbf{x}, \mathbf{y}) = \mathbf{v}^{(k)}(\mathbf{x}, \mathbf{y}).\mathbf{e}_j$. One should note that in absence of prescribed boundary conditions on the $x_3 = 0$ plane for the flows $(\mathbf{v}^{(k)}, p^{(k)})$ such a tensor **G** is not unique! For example, the usual (see Pozrikidis (1992)) free-space Oseen-Burgers tensor $\mathbf{G}^{\text{free}}$ and associated pressure field $p^{free,(k)}$ such that

$$8\pi\mu G_{jk}^{\text{free}}(\mathbf{x}, \mathbf{y}) = \frac{\delta_{jk}}{|\mathbf{x} - \mathbf{y}|} + \frac{[(\mathbf{x} - \mathbf{y}).\mathbf{e}_j][(\mathbf{x} - \mathbf{y}).\mathbf{e}_k]}{|\mathbf{x} - \mathbf{y}|^3}, \tag{7}$$

$$4\pi p^{free,(k)}(\mathbf{x}, \mathbf{y}) = (\mathbf{x} - \mathbf{y}).\mathbf{e}_k \tag{8}$$

is a solution to (4)-(6). The solution (7)-(8) is the so-called Stokeslet with strength $\mathbf{e}_k$ located at the pole **y**. The tensor $\mathbf{G}^{\text{free}}$ is weakly singular as the observation point **x** approaches the source point **y** and any Green tensor **G** actually takes the form $\mathbf{G} = \mathbf{G}^{\text{free}} + \mathbf{R}$ with **R** a tensor regular in the *entire* $x_3 > 0$ half-space. In contrast, the Green tensor $\mathbf{G}^c$ complying with the anisotropic slip condition (3) is unique and obtained from Stokes flows $(\mathbf{v}^{(k)}, p^{(k)})$ fulfilling (4)-(6) and the specific boundary

conditions (3) on the plane surface Σ, i. e. the additional relations

$$\mathbf{v}^{(k)}.\mathbf{e}_3 = 0 \;\; \text{on } \Sigma(x_3 = 0), \tag{9}$$

$$\mathbf{v}^{(k)}.\mathbf{e}_1 = b_1 \frac{\partial \mathbf{v}^{(k)}.\mathbf{e}_1}{\partial x_3} \;\; \text{on } \Sigma(x_3 = 0), \tag{10}$$

$$\mathbf{v}^{(k)}.\mathbf{e}_2 = b_2 \frac{\partial \mathbf{v}^{(k)}.\mathbf{e}_2}{\partial x_3} \;\; \text{on } \Sigma(x_3 = 0) \tag{11}$$

with prescribed slip lengths $0 \le b_2 \le b_1$. In summary, the retained Green tensor $\mathbf{G}^c$ is obtained by determining three Stokes flows $(\mathbf{v}^{(k)}, p^{(k)})$ governed by (4)-(6) and (9)-(11). If we further consider two flows $(\mathbf{u}, p)$ and $(\mathbf{u}', p)'$ having stress tensors $\boldsymbol{\sigma}$ and $\boldsymbol{\sigma}'$ and subject to the boundary conditions (3) on the surface Σ it is clear that

$$\int_{\Sigma} \mathbf{u}.\boldsymbol{\sigma}'.\mathbf{n} dS = \int_{\Sigma} \mathbf{u}'.\boldsymbol{\sigma}.\mathbf{n} dS. \tag{12}$$

Mimicking the treatment employed in Pozrikidis (1992) for a no-slip boundary it is then straightforward to show that, because of the above relation (12) the selected Green tensor $\mathbf{G}^c$ admits the following symmetry propoerty

$$G^c_{kj}(\mathbf{y}, \mathbf{x}) = G^c_{jk}(\mathbf{x}, \mathbf{y}). \tag{13}$$

Before closing this subsection, let us outline that property (13) would not necessarily hold when prescribing at the plane wall Σ other boundary conditions than the selected anisotropic ones (9)-(11).

2.2   *Application to the Stokes flow about a migrating solid particle*

Since the determination of the Green tensor $\mathbf{G}^c$ in §3 requires some efforts it is worth briefly illustrating to which extent its knowledge nicely facilitates the accurate determination of the flow about a solid particle migrating and interacting with the unbounded slipping wall Σ. As illustrated in Fig. 2, the particle $\mathscr{P}$ has smooth surface S with unit outward normal $\mathbf{n}$ pointing into the liquid.

The particle has prescribed rigid-body velocity $\mathbf{u}_{rb}$ on its surface S and the fluid flows with pressure p and velocity $\mathbf{u}$ in the liquid domain $\mathscr{D}$. The Stokes flow $(\mathbf{u}, p)$ obeys in the domain $\mathscr{D}$ the equations (4)-(6) with δ_{3d} set to zero, the anisotropic boundary conditions (3) and the condition $\mathbf{u} = \mathbf{u}_{rb}$ on S. Adopting the usual tensor summation convention and exploiting the property (13), it is then possible to show that the velocity $\mathbf{u}$ field then admits in the entire liquid domain $\mathscr{D}$ the key integral representation

$$\mathbf{u}(\mathbf{x}).\mathbf{e}_j = -\int_S \mathbf{f}(\mathbf{y}).\mathbf{e}_k G^c_{jk}(\mathbf{x}, \mathbf{y}) dS(\mathbf{y}), \;\; \mathbf{x} \text{ in } \mathscr{D} \tag{14}$$
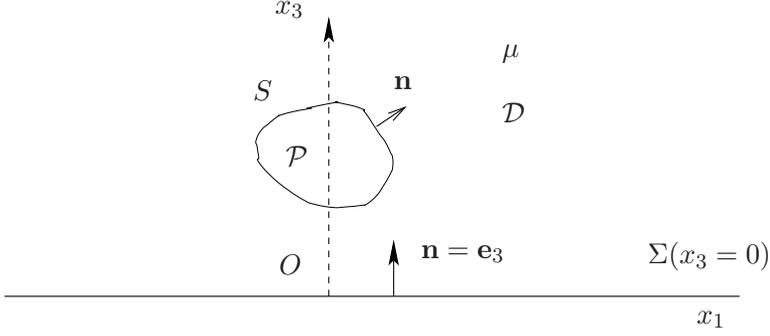
Figure 2: A *solid* and *arbitrarily-shaped* particle $\mathcal{P}$ near the $x_3 = 0$ motionless, impermeable, slipping and anisotropic plane boundary Σ.

with $\mathbf{f}$ the traction exerted by the flow $(\mathbf{u}, p)$ on the particle surface. One should note that (14) soleley involves the particle surface S (and not at all the unbounded boundary Σ) because the specific tensor $\mathbf{G}^c$ is employed! In addition, it actually reduces to a single-layer contribution because the particle has a rigid-body motion. Finally, letting the point $\mathbf{x}$ in (14) tend onto the surface S yields for the unknown surface traction $\mathbf{f}$ the key Fredholm boundary-integral equation of the first kind

$$\mathbf{u}_{rb}.\mathbf{e}_j = -\int_S \mathbf{f}(\mathbf{y}).\mathbf{e}_k G^c_{jk}(\mathbf{x}, \mathbf{y}) dS(\mathbf{y}), \ \mathbf{x} \text{ on } S. \tag{15}$$

Once $\mathbf{G}^c$ is determined, solving (15) then provides the vector $\mathbf{f}$ (and thus the net force and torque exerted by the flow on the particle) and also, if necessary and subsequently, the velocity field $\mathbf{u}$ about the particle by appealing to (14).

3 Determination of the Green tensor

This section obtains the required Green tensor Cartesian components $G^c_{jk}(\mathbf{x}, \mathbf{y})$ for arbitrary pole $\mathbf{y}$ and observation point $\mathbf{x}$ located above the plane surface Σ. It is recalled that, except for a few clearly specified cases, the usual tensor summation convention is used throughout this paper.

3.1 Employed decomposition and solution in the Fourier space

As shown in Fig. 1, we introduce the symmetric point $\mathbf{y}'$ of the selected pole $\mathbf{y}$ with respect to the plane, impermeable and slipping boundary Σ. Accordingly, $y'_3 = -y_3$ whereas $y'_i = y_i$ for $i = 1, 2$. For convenience, we also set $h = y_3$ and define the vectors $\mathbf{R} = \mathbf{x} - \mathbf{y} = R_i \mathbf{e}_i$ and $\mathbf{R}' = \mathbf{x} - \mathbf{y}' = R'_i \mathbf{e}_i$ such that $R'_1 = R_1, R'_2 = R_2, R_3 =$

$x_3 - h$ and $R'_3 = x_3 + h > 0$. For a given value of k we introduce the pressure field $p^{c,(k)}(\mathbf{x}, \mathbf{y})$ associated with the Stokes flow velocity $G^c_{jk}(\mathbf{x}, \mathbf{y})\mathbf{e}_j$ and, recalling the definitions (7)-(8), then adopt the following decompositions

$$G^c_{jk}(\mathbf{x}, \mathbf{y}) = G^{free}_{jk}(\mathbf{x}, \mathbf{y}) - G^{free}_{jk}(\mathbf{x}, \mathbf{y}') + w^{(k)}_j(\mathbf{x}, \mathbf{y}), \tag{16}$$

$$p^{c,(k)}(\mathbf{x}, \mathbf{y}) = p^{free,(k)}(\mathbf{x}, \mathbf{y}) - p^{free,(k)}(\mathbf{x}, \mathbf{y}') + s^{(k)}(\mathbf{x}, \mathbf{y}). \tag{17}$$

Hence, the flow $(G^c_{jk}(\mathbf{x}, \mathbf{y})\mathbf{e}_j, p^{c,(k)}(\mathbf{x}, \mathbf{y}))$ produced by a concentrated point with strength $\mathbf{e}_k$ at the source $\mathbf{y}$ is thus obtained by superposing a Stokeslet with strength $\mathbf{e}_k$ at $\mathbf{y}$, a Stokeslet with strength $-\mathbf{e}_k$ at the symmetric point $\mathbf{y}'$ and a Stokes flow with velocity $\mathbf{w}^{(k)} = w^{(k)}_j(\mathbf{x}, \mathbf{y})\mathbf{e}_j$ and pressure $s^{(k)}(\mathbf{x}, \mathbf{y})$. Since the Stokeslet located at $\mathbf{y}$ satifies (4), the third above flow is *regular in the entire half $x_3 > 0$ space*. Clearly, it obeys

$$\mu \nabla^2 \mathbf{w}^{(k)} = \nabla s^{(k)} \text{ and } \nabla . \mathbf{w}^{(k)} = 0 \text{ for } x_3 > 0, \tag{18}$$

$$(\mathbf{w}^{(k)}, s^{(k)}) \to (\mathbf{0}, 0) \text{ as } |\mathbf{x}| \to \infty \tag{19}$$

and, because the flow $G^c_{jk}(\mathbf{x}, \mathbf{y})\mathbf{e}_j$ satisfies the anisotropic slip condition (9)-(11), at the plane wall the additional impermeability condition

$$8\pi\mu w^{(k)}_3 = \delta_{k3}(\frac{1}{R'} - \frac{1}{R}) + \frac{R'_3 R'_k}{R'^3} - \frac{R_3 R_k}{R^3} \text{ at } x_3 = 0, \tag{20}$$

and the two anisotropic slip relations

$$8\pi\mu w^{(k)}_j + \delta_{jk}(\frac{1}{R} - \frac{1}{R'}) + \frac{R_j R_k}{R^3} - \frac{R'_j R'_k}{R'^3} =$$

$$b_j \left\{ 8\pi\mu \frac{\partial w^{(k)}_j}{\partial R'_3} + \delta_{jk}(\frac{R'_3}{R'^3} - \frac{R_3}{R^3}) + \delta_{k3}(\frac{R_j}{R^3} - \frac{R'_j}{R'^3}) \right.$$

$$\left. + 3(\frac{R'_j R'_k R'_3}{R'^5} - \frac{R_j R_k R_3}{R^5}) \right\} \text{ for } j = 1, 2 \text{ at } x_3 = 0 \tag{21}$$

where $R = |\mathbf{R}|, R = |\mathbf{R}'|$ and there is no summation over indices j in (21).

The problem (18)-(21) is solved here, using the two-dimensional Fourier transform $F<g>$ of a function g depending upon the variables R_1, R_2 and R'_3 defined as

$$F<g> = \hat{g}(\lambda_1, \lambda_2; R'_3)$$

$$= \frac{1}{2\pi} \int_{-\infty}^{\infty} \int_{-\infty}^{\infty} g(R_1, R_2, R'_3) e^{i(\lambda_1 R_1 + \lambda_2 R_2)} dR_1 dR_2 \tag{22}$$

with i the usual complex number such that $i^2 = -1$. Setting $\xi = \{\lambda_1^2 + \lambda_2^2\}^{1/2}$ and using Gradshteyn and Ryzhik (1963), one for example gets for $R_3' = x_3 + h > 0$ the identities

$$F<(R_1^2 + R_2^2 + R_3'^2)^{-1/2}> = \frac{e^{-R_3'\xi}}{\xi}, \tag{23}$$

$$F<(R_1^2 + R_2^2 + R_3'^2)^{-3/2}> = \frac{e^{-R_3'\xi}}{R_3'}. \tag{24}$$

From (18) the pressure field $s^{(k)}$ is harmonic in the entire $x_3 > 0$ domain where one therefore has the differential equation $\partial^2 \hat{s}^{(k)} / \partial R_3'^2 = \xi^2 \hat{s}^{(k)}$. Since the far-field behaviour (19) shows that $\hat{s}^{(k)}$ vanishes as $x_3 \to \infty$ the retained solution $\hat{s}^{(k)}$ thus reads

$$\hat{s}^{(k)} = \frac{h}{4\pi\mu} [2\mu B^{(k)}] e^{-\xi(R_3'-h)} \tag{25}$$

where the unknown function $B^{(k)}$ depends upon λ_1, λ_2, the length $h = y_3$ and the two slip lengths b_1 and b_2. In a similar fashion, the first equation (18) and the behaviour (19) also give the differential equation $\partial^2 \hat{w}_j^{(k)} / \partial R_3'^2 = \xi^2 \hat{w}_j^{(k)} + \hat{s}^{(k)}/\mu$ with $\hat{w}_j^{(k)}$ vanishing as $x_3 \to \infty$. Exploiting (25), the obtain solution takes the following form

$$\hat{w}_j^{(k)} = \frac{h}{4\pi\mu} \left\{ B_j^{(k)} + [i(\frac{\lambda_1 \delta_{1j} + \lambda_2 \delta_{2j}}{\xi}) + \delta_{j3}](R_3' - h)B^{(k)} \right\} e^{-(R_3'-h)\xi} \tag{26}$$

with three additional unknown functions $B^{(k)}$ still depending upon $(\lambda_1, \lambda_2, h, b_1)$ and b_2. Finally, one also gets the additional relation

$$B^{(k)} = i\lambda_1 B_1^{(k)} + i\lambda_2 B_2^{(k)} + \xi B_3^{(k)} \tag{27}$$

here obtained by enforcing the divergence-free condition required in (18). The four unknown functions $B^{(k)}, B_j^{(k)}$ are finally determined by using the Fourier tranforms of the boundary conditions (20)-(21). Appealing to (23)-(24) and noting that $R' =$

$R, R'_3 = h = -R_3$ at the plane surface $\Sigma(x_3 = 0)$ then easily shows that

$$B_3^{(k)} = i(\lambda_1 \delta_{1k} + \lambda_2 \delta_{1k}) g_1(\xi), \tag{28}$$

$$B_j^{(k)} - i\delta_{k3}(\lambda_1 \delta_{1j} + \lambda_2 \delta_{2j}) g_1(\xi) = b_j \Bigg\{$$

$$\frac{i(\lambda_1 \delta_{1j} + \lambda_2 \delta_{2j})}{\xi} B^{(k)} - \xi B_j^{(k)} + 2\delta_{jk} g_3(\xi)$$

$$-\lambda_j \lambda_k (1 - \delta_{k3}) a_1^j g_1(\xi) \Bigg\} \quad \text{for } j = 1, 2 \tag{29}$$

$$g_1(\xi) = \frac{e^{-h\xi}}{\xi}, \; g_3(\xi) = \frac{e^{-h\xi}}{h}. \tag{30}$$

As in (21), there is no summation over indices j in (29). Using the Maple Software to solve the linear system (27)-(29) then yields for $k = 3$ the solutions

$$B_1^{(3)} = \frac{i\lambda_1 g_1(\xi)[b_2\xi^2 + \xi + (b_2 - b_1)\lambda_2^2]}{2\xi^3 b_1 b_2 + (b_2 + 2b_1)\xi^2 + \xi + (b_2 - b_1)\lambda_2^2}, \tag{31}$$

$$B_2^{(3)} = \frac{i\lambda_2 g_1(\xi)[(2b_1 - b_2)\xi^2 + \xi + (b_2 - b_1)\lambda_2^2]}{2\xi^3 b_1 b_2 + (b_2 + 2b_1)\xi^2 + \xi + (b_2 - b_1)\lambda_2^2}, \tag{32}$$

$$B_3^{(3)} = 0, \tag{33}$$

$$B^{(3)} = -\frac{g_1(\xi)\xi^2[b_2\xi^2 + \xi + (b_1 - b_2)\lambda_2^2]}{2\xi^3 b_1 b_2 + (b_2 + 2b_1)\xi^2 + \xi + (b_2 - b_1)\lambda_2^2} \tag{34}$$

and for $k = 1$ the more heavy results

$$B_1^{(1)} = -\frac{2b_1[b_2 g_1(\xi)\xi^4 + g_1(\xi)\xi^3}{2b_1 b_2\xi^3 + (b_2 + 2b_1)\xi^2 + \xi + (b_2 - b_1)\lambda_2^2}$$

$$-\frac{b_2\xi^2(g_3(\xi) + g_1(\xi)\lambda_2^2)}{2b_1 b_2\xi^3 + (b_2 + 2b_1)\xi^2 + \xi + (b_2 - b_1)\lambda_2^2}$$

$$-\frac{g_1(\xi)\xi\lambda_2^2 + g_3(\xi) + b_2 g_3(\xi)\lambda_2^2]}{2b_1 b_2\xi^3 + (b_2 + 2b_1)\xi^2 + \xi + (b_2 - b_1)\lambda_2^2}, \tag{35}$$

$$B_2^{(1)} = -\frac{2b_2 \lambda_1 \lambda_2[b_1 g_1(\xi)\xi^2 + g_1(\xi)\xi + b_1 g_3(\xi)]}{2b_1 b_2\xi^3 + (b_2 + 2b_1)\xi^2 + \xi + (b_2 - b_1)\lambda_2^2}, \tag{36}$$

$$B_3^{(1)} = i\lambda_1 g_1(\xi), \tag{37}$$

$$B^{(1)} = \frac{i\lambda_1\xi[b_2 g_1(\xi)\xi^2 + (g_1(\xi) + 2b_1 b_2 g_3(\xi))\xi}{2b_1 b_2\xi^3 + (b_2 + 2b_1)\xi^2 + \xi + (b_2 - b_1)\lambda_2^2}$$

$$+\frac{i\lambda_1\xi[2b_1 g_3(\xi) + (b_1 - b_2)g_1(\xi)\lambda_2^2]}{2b_1 b_2\xi^3 + (b_2 + 2b_1)\xi^2 + \xi + (b_2 - b_1)\lambda_2^2}. \tag{38}$$

Of course, the functions $B_1^{(2)}, B_2^{(2)}, B_3^{(2)}$ and $B^{(2)}$ are obtained by replacing upperscripts (1) with (2) and switching subscripts 1 and 2 in (35)-(38). As announced, the functions $B^{(k)}, B_j^{(k)}$ depend upon $(\lambda_1, \lambda_2, h, b_1, b_2)$ and the results (31)-(38) permit one to gain the results in the Fourier space for the velocity components $\hat{w}_j^{(k)}$ and the pressure field $\hat{s}^{(k)}$.

3.2 Cartesian components of the Green tensor

The next key step consists in applying the inverse two-dimensional Fourier transform to the quantities $\hat{w}_j^{(k)}$ and (if also needed) $\hat{s}^{(k)}$ calculated in the previous subsection §3.1. By virtue of (22), one actually has the relation

$$g(R_1, R_2, R_3') = \frac{1}{2\pi} \int_{-\infty}^{\infty} \int_{-\infty}^{\infty} \hat{g}(\lambda_1, \lambda_2; R_3') e^{-i(\lambda_1 R_1 + \lambda_2 R_2)} d\lambda_1 d\lambda_2. \tag{39}$$

Restricting henceforth our attention to the velocity components, one then arrives at

$$w_j^{(k)} = \frac{h}{8\mu\pi^2} \int_{-\infty}^{\infty} \int_{-\infty}^{\infty} H_j^{(k)} e^{-R_3'\xi} e^{-i(\lambda_1 R_1 + \lambda_2 R_2)} d\lambda_1 d\lambda_2 \tag{40}$$

with functions $H_j^{(k)}$ deduced from (26), (31)-(38) and displayed in Appendix A.

3.3 Case of the isotropic Navier boundary condition

For this case we set $b = b_1 = b_2 \geq 0$ and the functions D and $H_j^{(k)}$ defined in the Appendix A then take simple forms with $D = \xi(1 + b\xi)(1 + 2b\xi)$. Employing the identities (see Gradshteyn and Ryzhik (1963))

$$\int_0^{2\pi} e^{-ix\cos\theta'} d\theta' = 2\pi J_0(x), \tag{41}$$

$$J_1(x) = -J_0'(x), \quad J_2(x) = 2J_1(x)/x - J_0(x), \tag{42}$$

$$\int_0^{\infty} \frac{J_0(ax)}{e^{cx}} dx = (a^2 + c^2)^{-1/2} \text{ for } a \geq 0 \text{ and } c > 0, \tag{43}$$

where J_m designates the usual Bessel function of integer order m and introducing the variable $\rho = \{R_1^2 + R_2^2\}^{1/2}$ makes it possible to cast the results (40) for $b = b_1 =$

b_2 into the following forms

$$w_j^{(3)} = (\frac{h}{4\pi\mu})(\frac{R_j}{\rho})\left\{L_1^{1,1} - x_3 L_1^{2,1}\right\} \text{ for } j = 1, 2, \tag{44}$$

$$w_3^{(3)} = -\frac{hx_3}{4\pi\mu}L_1^{2,0}, \tag{45}$$

$$w_1^{(1)} = \frac{h}{4\pi\mu}\left\{[2b + x_3(1 + 2b/h)][L_1^{2,2}(R_1/\rho)^2 - \frac{L_1^{1,1}}{\rho}]\right.$$
$$\left. + \frac{2b^2}{h\rho}L_2^{1,1} - L_2^{2,2}(R_2/\rho)^2 + \frac{2b}{h}L_1^{1,0}\right\}, \tag{46}$$

$$w_2^{(1)} = (\frac{h}{4\pi\mu})(\frac{R_1 R_2}{\rho^2})\left\{[x_3 + 2b(1 + x_3/h)]L_1^{2,2}\right.$$
$$\left. + \frac{2b^2}{h}L_2^{2,2}\right\}, \tag{47}$$

$$w_3^{(1)} = (\frac{h}{4\pi\mu})(\frac{R_1}{\rho})\left\{x_3(1 + 2b/h)L_1^{2,1}\right.$$
$$\left. + \frac{\rho}{(\rho^2 + R_3'^2)^{3/2}}\right\} \tag{48}$$

where the integrals $L_1^{p,q}$ and $L_2^{p,q}$ are defined for positive integers p and q as

$$L_1^{p,q} = \int_0^\infty \frac{\xi^p e^{-R_3'\xi} J_q(\rho\xi)d\xi}{1 + 2b\xi}, \tag{49}$$

$$L_2^{p,q} = \int_0^\infty \frac{\xi^p e^{-R_3'\xi} J_q(\rho\xi)d\xi}{(1 + b\xi)(1 + 2b\xi)}. \tag{50}$$

As a consequence, for $b_1 = b_2$ the task reduces to the computation of seven *one-dimensional* regular integrals: $L_1^{1,0}, L_1^{1,1}, L_1^{2,0}, L_1^{2,1}, L_1^{2,2}, L_2^{1,1}$ and $L_2^{2,2}$.

4 Advocated Numerical treatment and benchmark tests

As emphasized in the introduction, it is in practice both required to theoretically determine the Green tensor complying with the anisotropic slip condition (3) (see Issue 1) and accurately compute its Cartesian components at a reasonable cpu time cost (see Issue 2). While Issue 1 has been treated in §3 the present section copes with the Issue 2 by proposing, implementing and benchmarking a suitable numerical method to compute the velocity components $w_j^{(k)}$ given by (40) and the material displayed in Appendix A. As detailed in §4.1, the key point consists in rewriting the *two-dimensional* integrals $w_j^{(k)}$ as *one-dimensional* ones.

4.1 Advocated procedure to solely end up with one-dimensional integrals

As shown by (44)-(50), when $b_1 = b_2 = b$ one solely encounters *one-dimensional* integrals of the following form

$$I(\rho, x_3, h; b) = \frac{h}{4\pi\mu} \int_0^\infty e^{-R_3'\xi} S(\xi, \rho, x_3, h; b) d\xi \tag{51}$$

with S a smooth function of ξ and $R_3' = x_3 + h > 0$ so that $e^{-R_3'\xi}$ decays as ξ becomes large.

In constrast, for $b_1 > b_2 \geq 0$ the velocity component $w_j^{(k)}$ turns out to be a *fully two-dimensional integral* (recall (40)) which depends upon the selected pole $\mathbf{y}$, the observation point $\mathbf{x}$ and the two inequal positive slip lengths $b_1 > b_2$ through the variables $x_3, h = y_3, R_1 = x_1 - y_1, R_2 = x_2 - y_2$ and the sum $R_3' = x_3 + h > 0$. As seen in (40), the integrand has a regular (see (80)-(88)) and decaying term $H_j^{(k)} e^{-R_3'\xi}$ but also exhibits *oscillations* produced by the factor $e^{-i(\lambda_1 R_1 + \lambda_2 R_2)}$. At a very first glance, one thus might think about accurately and quickly compute each integral $w_j^{(k)}$ using the so-called Fast Fourier Transform (FFT) technique. Unfortunately, such a powerful procedure tremendously speeds up the calculations only when one is actually interested in *simultaneously* gaining the values of an oscillating integral at a large number of wave numbers (i. e. here at a large number of pairs (R_1, R_2) in the two-dimensional physical space). Because we are interested in calculating $w_j^{(k)}$ solely at one prescribed value (R_1, R_2) the FFT is not competitive for the present work. Fortunately, it has been found both possible and very efficient to *analytically perform* one integration in (40) therefore ending up with solely a one-dimensional integral to be computed (analogous to (51)) when handling $w_j^{(k)}$. The employed procedure is explained below and illustrated for the treatment of the component $w_2^{(1)}$ in §4.2.

As sketched in Fig. 3, we first introduce the polar coordinates $(\rho, \alpha), (\xi, \theta)$ and the angle θ' such that $\theta' \in [0, 2\pi]$ and

$$R_1 = \rho \cos\alpha, \quad R_2 = \rho \sin\alpha, \tag{52}$$
$$\lambda_1 = \xi \cos\theta, \quad \lambda_2 = \xi \sin\theta, \quad \theta = \theta' + \alpha. \tag{53}$$

Then $d\lambda_1 d\lambda_2 = \xi d\xi d\theta$ and the equality (40) becomes

$$w_j^{(k)} = \frac{h}{4\mu\pi} \int_0^\infty e^{-R_3'\xi} S_j^{(k)}(\xi, \rho, \alpha, x_3, h; b_1, b_2) d\xi \tag{54}$$

with $S_j^{(k)}$ a one-dimensional and *oscillating* integral of the following form

$$S_j^{(k)} = \frac{1}{2\pi} \int_0^{2\pi} e^{-\rho\xi \cos\theta'} T_j^{(k)}(\theta, \xi, x_3, h; b_1, b_2) d\theta' \tag{55}$$
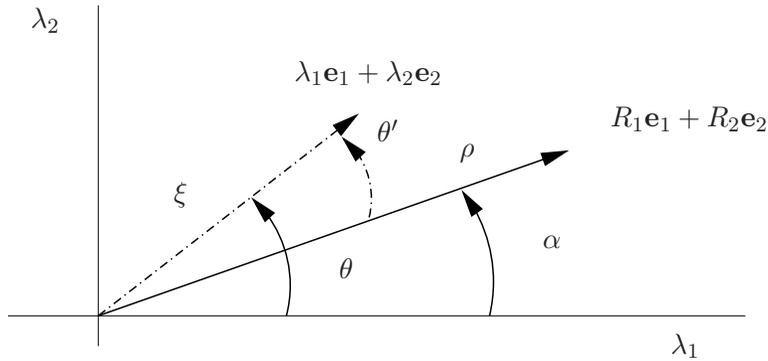
Figure 3: Adopted notations in the Fourier space with angles θ, θ' and variables ρ and ξ.

where it is recalled that $\theta = \theta' + \alpha$. As the reader may easily check, inspecting the definitions (80)-(88) shows that each fucntion $T_j^{(k)}$ actually consists of terms of the form $A(\theta)T$ with

$$A(\theta) = 1, \cos(\theta), \sin(\theta), \cos(2\theta), \sin(2\theta), \cos(4\theta), \tag{56}$$

$$T = c(\xi, x_3, h; b_1, b_2) + \frac{C(\xi, , x_3, h; b_1, b_2)}{1 - a^2(\xi; b_1, b_2)\sin^2(\theta)} \tag{57}$$

and, recalling that $b_1 \geq b_2$ and $\xi \geq 0$,

$$a(\xi; b_1, b_2) = \left[\frac{(b_1 - b_2)\xi}{2b_1 b_2 \xi^2 + (b_2 + 2b_1)\xi + 1}\right]^{1/2} < 1, \tag{58}$$

Accordingly, it is possible to rewrite T as a serie Fourier of the following type

$$T(\theta) = \sum_{n=0}^{\infty} t_n(\xi, x_3, h; b_1, b_2)\cos(2n\theta) \tag{59}$$

with coefficients c_n *analytically* obtained from the relations (see, for (61), Gradshteyn and Ryzhik (1963) page 368 for $a^2 < 1$)

$$t_n = \frac{2^{2-\delta_{n0}}}{\pi} \int_0^{\pi/2} T(\theta)\cos(2n\theta)d\theta, \tag{60}$$

$$\int_0^{\pi/2} \frac{\cos(2n\theta)d\theta}{1 - a^2\sin^2(\theta)} = \frac{\pi(-1)^n}{2\sqrt{1-a^2}}\left[\frac{1 - \sqrt{1-a^2}}{a}\right]^{2n}. \tag{61}$$

It follows that each term $A(\theta)T$ becomes

$$A(\theta)T = \sum_{n=0}^{\infty} t_n(\xi, x_3, h; b_1, b_2) A(\theta' + \alpha)$$
$$[\cos(2n\alpha)\cos(2n\theta') - \sin(2n\alpha)\sin(2n\theta')]. \tag{62}$$

Developing the function $A(\theta' + \alpha)$ in terms of the functions $1, \cos(\theta'), \sin(\theta'), \cos(2\theta')$ and $\sin(2\theta')$ [1] and exploiting the following identities

$$\int_0^{2\pi} e^{-i\rho\xi\cos\theta'}\cos(2n\theta')d\theta' = 2\pi(-1)^n J_{2n}(\rho\xi), \tag{63}$$

$$\int_0^{2\pi} e^{-i\rho\xi\cos\theta'}\sin(2n\theta')d\theta' = 0, \tag{64}$$

$$i\int_0^{2\pi} e^{-i\rho\xi\cos\theta'}\cos(2n\theta')\cos(\theta')d\theta' = pi\sin[(n+\frac{1}{2})\pi]J_{2n+1}(\rho\xi)$$
$$+\pi\sin[|n-\frac{1}{2}|\pi]J_{|2n-1|}(\rho\xi), \tag{65}$$

$$i\int_0^{2\pi} e^{-i\rho\xi\sin\theta'}\sin(2n\theta')\sin(\theta')d\theta' = \pi\sin[|n-\frac{1}{2}|\pi]J_{|2n-1|}(\rho\xi)$$
$$-\pi\sin[(n+\frac{1}{2})\pi]J_{2n+1}(\rho\xi)\}, \tag{66}$$

$$\int_0^{2\pi} e^{-i\rho\xi\cos\theta'}\cos(2n\theta')\cos(2\theta')d\theta' =$$
$$\pi(-1)^{n+1}\{J_{2n+2}(\rho\xi) + J_{|2n-2|}(\rho\xi)\}, \tag{67}$$

$$\int_0^{2\pi} e^{-i\rho\xi\cos\theta'}\sin(2n\theta')\sin(2\theta')d\theta' =$$
$$\pi(-1)^{n+1}\{J_{|2n-2|}(\rho\xi) - J_{2n+2}(\rho\xi)\}, \tag{68}$$

then makes it possible to analytically perform the calculation of the *oscillating* integral $S_j^{(k)}$ defined by (55). More precisely, the quantity $S_j^{(k)}$ then admits the expansion

$$S_j^{(k)}(\xi, \rho, \alpha, x_3, h; b_1, b_2) = \sum_{n=0}^{\infty} s_n(\xi, \rho, \alpha, x_3, h; b_1, b_2) \tag{69}$$

with each "coefficient" s_n analytically determined and if necessarily computed at any desired accuracy level at a very low cpu time cost. Of course, when $b_1 = b_2 = b$ the coefficients t_n in (62) and s_n in (69) vanish for $n \geq 1$ and the value of $s_0(\xi, \rho, \alpha, x_3, h; b_1, b_2)$ retrieves the one deduced from (44)-(50).

---

[1] When $A(\theta) = \cos(4\theta)$ we actually directly write the product $A(\theta)T(\theta)$ as a Fourier serie (59).

In summary, the numerical implementation obtains the velocity $w_j^{(k)}$ by computing the *one-dimensional* (54) once the occurring function $S_j^{(k)}$ is numerically and accurately known truncating its *analytical expansion* (69).

4.2 Illustrating example for $w_2^{(1)}$

The procedure introduced in §4.1 in order to arrive at the key expansion (69) for each component $w_j^{(k)}$ solely requires elementary manipulations which are however too long to be reproduced here for each value for the pair (j,k). Nevertheless, it is worth detailing for one example. This is achieved in this subsection by adressing the component $w_2^{(1)}$.

Using the relations $d\lambda_1 d\lambda_2 = \xi d\xi d\theta'$, $\lambda_1 \lambda_2 = \xi^2 \sin(2\theta)/2$ and the definition (84) of the function $H_2^{(1)}$ then yields $T_2^{(1)} = \sin(2\theta)T$ with function $T_2^{(1)}$ introduced by (55) and here such that

$$T = \frac{\xi^2 x_3}{2} + \frac{[-Q_2^{(1)}(\xi, x_3, h; b_1, b_2)\xi^2/2]}{1 - a^2(\xi; b_1, b_2)\sin^2(\theta)}, \tag{70}$$

$$Q_2^{(1)} = \frac{N}{2\xi^2 b_1 b_2 + (b_2 + 2b_1)\xi + 1}, \tag{71}$$

$$N = 2b_2(1 + b_1\xi + b_1/h) + x_3[1 + (b_2 + 2b_1)\xi \\ + 2b_1 b_2\xi^2 + (1 + b_2\xi)(1 + 2b_1/h)]. \tag{72}$$

Appealing to (60)-(61), it immediately follows that (59) here holds for

$$t_0 = \frac{\xi^2}{2}[x_3 - \frac{Q_2^{(1)}}{\sqrt{1-a^2}}], \tag{73}$$

$$t_n = \frac{(-1)^n \xi^2 Q_2^{(1)}}{\sqrt{1-a^2}}[\frac{1-\sqrt{1-a^2}}{a}]^{2n} \quad \text{for } n \geq 1. \tag{74}$$

Exploiting the relation $\theta = \theta' + \alpha$, the resulting identities

$$\sin(2\theta) = \sin(2\alpha)\cos(2\theta') + \cos(2\alpha)\sin(2\theta'), \tag{75}$$

$$\cos(2\theta) = \cos(2\alpha)\cos(2\theta') - \sin(2\alpha)\sin(2\theta'), \tag{76}$$

and the relations (67)-(68) one thus deduces that function $S_2^{(1)}$ occurring in (54) and obtained from $T_2^{(1)}$ by performing the integration over θ' as shown in (55) admit

the following *analytical* expansion

$$S_2^{(1)} = -t_0 \sin(2\alpha) J_2(\rho\xi) + \sum_{n\geq 1} [\frac{t_n}{2}] \Big\{ \sin[(2n+2)\alpha](-1)^{n+1} J_{2n+2}(\rho\xi)$$

$$-\sin[(2n-2)\alpha](-1)^{n-1} J_{2n-2}(\rho\xi) \Big\} \tag{77}$$

with t_n given for $n \geq 0$ by (71)-(74).

4.3 Numerical treatment of each encountered one-dimensional integral and benchmark tests

One-dimensional integrals (51) and (54) are computed using the change of variable $\xi = -\log t$. For instance, for (54) one then gets

$$\int_0^\infty e^{-R_3'\xi} S_j^{(k)}(\xi, \rho, \alpha, x_3, h; b_1, b_2) d\xi = \int_0^1 t^{R_3'-1} S_j^{(k)}(-\log t, \rho, \alpha, x_3, h; b_1, b_2) dt \tag{78}$$

and the regular integral on the right-hand side of (78) is here accurately and iteratively calculated at a given accuracy level by first truncating the expansion (69) at this prescribed accuracy and then iteratively dividing the domain $[0,1]$ into equal subsegments on which a Gaussian of order 8 or 16 is employed.

Table 1: Comparisons against the results provided by the Maple Software for settings $b_1 = 1, b_2 = 0.2, x_3 = 1/2$ and $y_3 = h = 1/3$. Case of *weakly-oscillating* integrals: $R_1 = -0.7, R_2 = -0.1$ It is recalled that $w_j^{(k)} = h w_j'^{(k)}/(4\pi\mu)$.

$w_j'^k$	Maple ($R_3' = 0.1$)	Fortran ($R_3' = 0.1$)	Maple ($R_3' = 1$)	Fortran ($R_3' = 1$)
$w_1'^1$	7.7567698098	7.7567698219	1.1727368380	1.1727368385
$w_2'^1$	1.5644810076	1.5644810085	0.0717101966	0.0717101967
$w_3'^1$	-5.5551541286	-5.5551541469	-0.9636199432	-0.963199432
$w_1'^2$	1.4449074993	1.4449075005	0.0652592911	0.0652592913
$w_2'^2$	-2.7285236646	-2.7285236672	0.0512840044	0.0512840044
$w_3'^2$	-0.8762725769	-0.8762725744	-0.1164679197	-0.1164679200
$w_1'^3$	0.8312453930	0.8312453953	0.0438230004	0.0438230005
$w_2'^3$	0.2527838614	0.2527838601	-0.0037009441	-0.0037009441
$w_3'^3$	-0.5668804764	-0.5668804827	-0.1761637586	-0.1761637584

Table 2: Comparisons against the results provided by the Maple Software for settings $b_1 = 1, b_2 = 0.2, x_3 = 1/2$ and $y_3 = h = 1/3$. Case of *moderately-oscillating* integrals: $R_1 = 2, R_2 = -1.5$. It is recalled that $w_j^{(k)} = hw_j^{'(k)}/(4\pi\mu)$.

$w_j^{'k}$	Maple ($R_3' = 0.1$)	Fortran ($R_3' = 0.1$)	Maple ($R_3' = 1$)	Fortran ($R_3' = 1$)
$w_1^{'1}$	0.3536712338	0.35367122374	0.3544786109	0.3544786084
$w_2^{'1}$	-0.2896394410	-0.02896394436	-0.1463434884	-0.1463434884
$w_3^{'1}$	0.1970021000	0.1970020930	0.1927649466	0.1927649460
$w_1^{'2}$	-0.2516197474	-0.2516197506	-0.1280063049	-0.1280063049
$w_2^{'2}$	0.0603747621	0.0603747626	0.0616010126	0.0616010125
$w_3^{'2}$	-0.0150214943	-0.150214943	-0.1216560698	-0.1216560697
$w_1^{'3}$	0.0809436825	0.0809436814	0.0384483781	0.0384483782
$w_2^{'3}$	-0.0487071456	-0.0487071403	-0.0393437158	-0.0393437158
$w_3^{'3}$	0.0162356781	0.0162356779	0.0004864529	0.0004864529

Table 3: Comparisons against the results provided by the Maple Software for settings $b_1 = 1, b_2 = 0.2, x_3 = 1/2$ and $y_3 = h = 1/3$. Case of *strongly–oscillating* integrals: $R_1 = 20, R_2 = -15$. It is recalled that $w_j^{(k)} = hw_j^{'(k)}/(4\pi\mu)$.

$w_j^{'k}$	Maple ($R_3' = 0.2$)	Fortran ($R_3' = 0.2$)	Maple ($R_3' = 1$)	Fortran ($R_3' = 1$)
$w_1^{'1}$	0.0010074508	0.0010074599	0.0012990282	0.0012990271
$w_2^{'1}$	-0.0004836719	-0.0004836679	-0.0004759370	-0.0004759400
$w_3^{'1}$	0.0013060891	0.0013060910	0.0013194533	0.0013194532
$w_1^{'2}$	-0.0004085189	-0.0004085246	-0.00004020889	-0.00004020880
$w_2^{'2}$	0.0000592200	0.0000592200	0.0001181210	0.0001181210
$w_3^{'2}$	-0.0009749514	-0.0009749424	-0.0009764560	-0.0009764560
$w_1^{'3}$	0.0012618453	0.0012618460	0.0012472237	0.0012472255
$w_2^{'3}$	-0.0009469234	-0.0009468681	-0.0009416822	-0.0009416821
$w_3^{'3}$	0.0000313950	0.0000313952	0.0000306379	0.0000306376

Comparisons against the Maple Sofware are provided for the auxiliary quantity $w_j^{'(k)} = 4\pi\mu w_j^{(k)}/h$ (see (54)) in Tables 1, 2, 3 for $x_3 = 1/2$ and $h = 1/3$ and several values of the parameter $R_3' > 0$ (here selected as if independent of $x_3 + h$) and of the pair (R_1, R_2) which dictates the magnitude of the oscillating factor in (39). The Maple Software directly computes the formula (40) at a required 10^{-10} accu-

racy (increasing the required accuracy results in a large computational time for the Maple Software). The same accuracy level has been set in our numerical computations and the obtained results perfectly match the ones predicted by the Maple Software. In any case, our numerical treatment is very fast compared with the Maple Software which was also found to becomes very slow for strong oscillations (see Table 3) and R_3 weak. This is the reason why the lower employed of R'_3 in Table 3 is equal to 0.2 (whereas Tables 1 and 2 report comparisons for $R'_3 = 0.1$). It was also found in our numerical code that, as expected, the cpu time cost for anisotropic case $b1 \neq b_2$ is comparable with the cpu time cost for the isotropic case $b_1 = b_2$.

5 Concluding remarks

The Green tensor for an extended and anisotropic slip condition at a plane, motionless, impermeable and slipping wall has been theoretically obtained. An efficient and accurate numerical implementation has been also proposed to calculate at a reasonable cpu time cost and a sufficient accuracy level each Cartesian component of the derived Green tensor and the achieved comparisons against the Maple Software clearly show that the advocated numerical strategy provides very good results.

This work opens the way to the challenging investigation of the motion of a solid particle suspended in a liquid bounded by such a non-isotropic slipping surface. The use of the proposed Green tensor will make it possible to deal with the case of a non-necessarily spherical particle by resorting to a boundary-integral method. Such a key issue however requires many additional efforts and is therefore postponed to a future work.

Finally, the present paper is dedicated to our outstanding colleague Professor Wilson Sergio Venturini who sadly passed away on 15th July, 2010 at the age of 62.

References

Baudry, J.; Charlaix, E.; Tonck, A.; Mazuyer, D. (2001): Experimental evidence for a large slip effect at a nonwetting fluid-solid interface. *Langmuir*, vol. 17, pp. 5232–5236.

Bazant, M.; Vinagradova, O. I. (2008): Tensorial hydrodynamic slip. *J. Fluid Mech.*, vol. 613, pp. 125–134.

Bhattacharya, S.; Bławzdziewicz, J.; Wajnryb, E. (2005): Hydrodynamic interactions of spherical particles in suspensions confined between two planar walls. *J. Fluid Mech.*, vol. 541, pp. 263–292.

Blake, J. R. (1971):   A note on the image system for a stokeslet in a no-slip boundary. *Proc. Camb. Phil. Soc.*, vol. 70, pp. 303–310.

Brenner, H. (1961):   The slow motion of a sphere through a viscous fluid towards a plane surface. *Chemical Engineering Science*, vol. 16, pp. 242–251.

Churaev, N.; Sobolev, V.; Somov, A. N. (1994):   Slippage of liquids over lyophobic solid surfaces. *J. Colloid Int. Sci.*, vol. 97, pp. 574–581.

Cichocki, B.; Felderhof, B. U.; Hinsen, K.; Wajnryb, E.; Błаwzdziewicz, J. (1994):   Friction and mobility of many spheres in Stokes flow.   *J. Chem. Phys.*, vol. 100, pp. 3780–3790.

Cichocki, B.; Jones, R. B. (1998):   Image representation of a spherical particle near a hard wall. *Physica A*, vol. 258, no. 112, pp. 273–302.

Cichocki, B.; Jones, R. B.; Kutteh, R.; Wajnryb, E. (2000):   Friction and mobility for colloidal spheres in stokes flow near a boundary. *J. Chem. Phys.*, vol. 112, no. 5, pp. 2548–2561.

Cooley, M. D. A.; O'Neill, M. E. (1969):   On the slow motion generated in a viscous fluid by the approach of a sphere to a plane wall or stationary sphere. *Mathematika*, vol. 16, pp. 37–49.

Davis, A.; Kezirian, M.; Brenner, H. (1994):   On the stokes-einstein model of surface diffusion along solid surfaces: Slip boundary conditions.   *J.Colloid Interface Sci.*, vol. 1065, pp. 129–140.

Dean, W. R.; O'Neill, M. E. (1963):   A slow rotation of viscous liquid caused by the rotation of a solid sphere. *Mathematika*, vol. 10, pp. 13–24.

Ekiel-Jeżewska, M. L.; Wajnryb, E. (2009):   Hydrodynamic interactions between spherical particles in Stokes flow by the multipole method. In Feuillebois, F.; Sellier, A.(Eds): *Theoretical Methods for micro-scale viscous flows*. Transorld Research Network. ISBN:978-81-7985-400-4.

Feuillebois, F. (1989):   Some theoretical results for the motion of solid spherical particles in a viscous fluid. In Hewitt, G. F.; Delhaye, J. M.; Zuber, N.(Eds): *Multiphase Science and Technology, volume 4*, pp. 583–798. Hemisphere Publishing Co, New York.

Feuillebois, F.; Loussaief, H.; Pasol, L. (2009):   Particles in creeping flow near a slip wall. In Todorov, M. D.; Christov, C. I.(Eds): *Applications of Mathematics in Technical and Natural Sciences*, pp. 3–14. American Institute of Physics.

Gradshteyn, I.; Ryzhik, I. M. (1963):   *Tables of integrals, series, and products*. Academic Press, 1963.

Happel, J.; Brenner, H. (1991): *Low Reynolds number hydrodynamics*. Kluwer Academic Publishers, Dordrecht, Boston, London.

Hsu, R.; Ganatos, P. (1989): The motion of a rigid body in viscous fluid bounded by a plane wall. *J. Fluid Mech*, vol. 207, pp. 29–72.

Hsu, R.; Ganatos, P. (1994): Gravitational and zero-drag motion of a spheroid adjacent to an inclined plane at low Reynolds number. *J. Fluid Mech*, vol. 268, pp. 267–292.

Jones, R. (2004): Spherical particle in Poiseuille flow between planar walls. *J. Chem. Phys.*, vol. 121, no. 1, pp. 483–500.

Jones, R. (2009): Dynamics of a colloid in a spherical cavity. In Feuillebois, F.; Sellier, A.(Eds): *Theoretical Methods for micro-scale viscous flows*. Transorld Research Network. ISBN:978-81-7985-400-4.

Kim, S.; Karrila, S. (1991): *Microhydrodynamics: Principles and Selected Applications*. Butterworth-Heinemann.

Ladyzhenskaya, O. A. (1969): *The Mathematical Theory of Viscous Incompressible Flow*. Gordon & Breach.

Liron, N.; Mochon, S. (1976): Stokes flow for a stokeslet between two parallel flat plates. *J. Eng. Math.*, vol. 10, no. 4, pp. 287–303.

Liron, N.; Shahar, R. (1978): Stokes flow due to a stokeslet in a pipe. *J. Fluid Mech.*, vol. 86, pp. 727–744.

Lorenz, H. A. (1907): Ein allgemeiner satz, die bewegung einer reibenden flussigkeit betreffend, nebst einigen anwendungen desselben. *Abhand. Theor. Phys.*, vol. 1, pp. 23–42.

Maude, A. D. (1961): End effects in a falling-sphere viscometer. *British J. of Appl. Physics*, vol. 12, pp. 293–295.

Miyazaki, T.; Hasimoto, H. (1978): The motion of a small sphere in fluid near a circular hole in a plane wall. *J. Fluid Mech.*, vol. 145, pp. 201–221.

Navier, C. L. M. H. (1823): Mémoire sur les lois du mouvement des fluides. *Mémoire de l'Académie Royale des Sciences de l'Institut de France*, vol. 6, pp. 389–440.

O'Neill, M. E. (1964): A slow motion of viscous liquid caused by a slowly moving solid sphere. *Mathematika*, vol. 11, pp. 67–74.

O'Neill, M. E. (1967): A slow motion of viscous liquid caused by a slowly moving solid sphere: an addendum. *Mathematika*, vol. 14, pp. 170–172.

O'Neill, M. E. (1968):   A sphere in contact with a plane wall in a slow linear shear flow. *Chemical Engineering Science*, vol. 23, pp. 1293–1298.

O'Neill, M. E. (1969):   On asymmetrical slow viscous flows caused by the motion of two equal spheres almost in contact. *Proc. Camb. Phil. Soc.*, vol. 65, pp. 543–555.

O'Neill, M. E.; Bhatt, B. S. (1991):   Slow motion of a solid sphere in the presence of a naturally permeable surface. *Q. J. Mech. Appl. Math.*, vol. 44, pp. 91–104.

Oseen, C. W. (1927):   *Neure Methoden und Ergebnisse in der Hydrodynamik.* Akademische Verlagsgesellschat M. B. H.

Pasol, L.; Sellier, A.; Feuillebois, F. (2010):   Creeping flow around a solid sphere in the vicinity of a plane solid wall. In Feuillebois, F.; Sellier, A.(Eds): *Theoretical Methods for small scale viscous flows*. Transworld Research Network. ISBN: 978-81-7895-400-4.

Pozrikidis, C. (1992):   *Boundary integral and singularity methods for linearized viscous flow*. Cambridge University Press.

Sellier, A. (2008):   Slow viscous motion of a solid particle in a spherical cavity. *CMES: Computer Modeling in Engineering & Sciences*, vol. 25, no. 3, pp. 165–179.

Sellier, A.; Pasol, L. (2006):   Sedimentation of a solid particle immersed in a fluid film. *CMES: Computer Modeling in Engineering & Sciences*, vol. 16, no. 3, pp. 187–196.

Stimson, M.; Jeffery, G. B. (1926):   The motion of two spheres in a viscous Fluid. *Proc. Roy. Soc.*, vol. A 111, pp. 110–121.

Stone, H.; Stroock, A. D.; Adjari, A. (2004):   Slippage of liquids over lyophobic solid surfaces. *Annu. Rev. Fluid Mech.*, vol. 36, pp. 381–411.

Youngren, G. K.; Acrivos, A. (1975):   Stokes flow past a particle of arbitrary shape: a numerical method of solution. *J. Fluid Mech.*, vol. 69, no. 2, pp. 377–403.

Youngren, G. K.; Acrivos, A. (1976):   Stokes flow past a particle of arbitrary shape: a numerical method of solution. Corrigendum. *J. Fluid Mech.*, vol. 75, pp. 813.

Appendix A: Functions $H_j^{(k)}$

This Appendix provides the functions $H_j^{(k)}$ arising in (38). Upon introducing the function D as

$$
\begin{aligned}
D &= 2\xi^3 b_1 b_2 + (b_2 + 2b_1)\xi^2 + \xi + (b_2 - b_1)\lambda_2^2 \\
&= 2\xi^3 b_1 b_2 + (b_1 + 2b_2)\xi^2 + \xi + (b_1 - b_2)\lambda_1^2
\end{aligned}
\tag{79}
$$

and exploiting the definitions (30) and the results (31)-(38), one easily gets

$$H_1^{(3)} = \frac{i\lambda_1}{D}\Big\{b_2\xi + 1 + (b_2 - b_1)\lambda_2^2/\xi$$
$$-x_3[b_2\xi^2 + \xi + (b1 - b_2)\lambda_2^2]\Big\}, \tag{80}$$

$$H_2^{(3)} = \frac{i\lambda_2}{D}\Big\{(2b_1 - b_2)\xi + 1 + (b_2 - b_1)\lambda_2^2/\xi$$
$$-x_3[b_2\xi^2 + \xi + (b1 - b_2)\lambda_2^2], \tag{81}$$

$$H_3^{(3)} = -\frac{\xi x_3}{D}\Big\{b_2\xi^2 + \xi + (b1 - b_2)\lambda_2^2\Big\}, \tag{82}$$

$$H_1^{(1)} = -\frac{1}{D}\Big\{2b_1\xi(\xi - 1/h)(1 + b_2\xi)$$
$$-2b_1(1 + b_2\xi + b_2/h)\lambda_2^2$$
$$+\lambda_1^2 x_3[(1 + b_2\xi)(1 + 2b_1/h) + (b_1 - b_2)\lambda_2^2/\xi]\Big\}, \tag{83}$$

$$H_2^{(1)} = -\frac{\lambda_1\lambda_2}{D}\Big\{2b_2(b_1\xi + 1 + b_1/h)$$
$$+x_3[(1 + b_2\xi)(1 + 2b_1/h) + (b_1 - b_2)\lambda_2^2/\xi]\Big\}, \tag{84}$$

$$H_3^{(1)} = \frac{i\lambda_1}{D}\Big\{D/\xi$$
$$+x_3\xi[(1 + b_2\xi)(1 + 2b_1/h) + (b_1 - b_2)\lambda_2^2/\xi]\Big\} \tag{85}$$

$$H_1^{(2)} = -\frac{\lambda_1\lambda_2}{D}\Big\{2b_1(b_2\xi + 1 + b_2/h)$$
$$+x_3[(1 + b_1\xi)(1 + 2b_2/h) + (b_2 - b_1)\lambda_1^2/\xi]\Big\}, \tag{86}$$

$$H_2^{(2)} = -\frac{1}{D}\Big\{2b_2\xi(\xi - 1/h)(1 + b_1\xi)$$
$$-2b_2(1 + b_1\xi + b_1/h)\lambda_1^2$$
$$+\lambda_2^2 x_3[(1 + b_1\xi)(1 + 2b_2/h) + (b_2 - b_1)\lambda_1^2/\xi]\Big\}, \tag{87}$$

$$H_3^{(2)} = \frac{i\lambda_2}{D}\Big\{D/\xi$$
$$+x_3\xi[(1 + b_1\xi)(1 + 2b_2/h) + (b_2 - b_1)\lambda_2^2/\xi]\Big\}. \tag{88}$$